Cooperatively Generated Stresslet Flows Supply Fresh Fluid to Multicellular Choanoflagellate Colonies

Marcus Roper, Mark J. Dayel, Rachel E. Pepper, and M. A. R. Koehl

Phys. Rev. Lett. **110**, 228104 — Published 31 May 2013

DOI: 10.1103/PhysRevLett.110.228104

Cooperatively generated stresslet flows supply fresh fluid to multicellular choanoflagellate colonies.

Marcus Roper,[1] Mark J. Dayel,[2] Rachel E. Pepper,[3,4] and M.A.R. Koehl[3]

[1] *Dept. of Mathematics, UCLA, Los Angeles, CA 90095*
[2] *Molecular and Cellular Biology, UC Berkeley, CA 94720*
[3] *Integrative Biology, UC Berkeley, CA 94720*
[4] *Civil and Environmental Engineering, UC Berkeley, CA 94720*

(Dated: May 3, 2013)

The flagellated protozoan *Salpingoeca rosetta* is one of the closest relatives of multicellular animals. Unicellular *S. rosetta* can be induced to form multicellular colonies, but colonies swim slower than individual cells so the advantages conferred by colony formation are uncertain. Here we use theoretical models to show that hydrodynamic cooperation between cells can increase the fluid supply to the colony, an important predictor of feeding rate. Our results suggest that hydrodynamic benefits may have been an important selective factor in the evolution of early multicellular animals.

PACS numbers: 47.63.-b, 87.18.Fx, 87.16.Qp

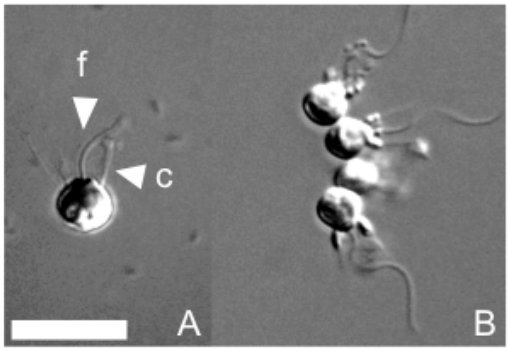

FIG. 1. Multi- and uni-cellular stages in the life history of *S. rosetta*. (A) Under a broad variety of growth conditions, cells are planktonic and either freely swimming or attached to substrates. A flagellum (f) propels freely swimming cells through water and creates flows from which prey are captured on a collar of microvilli (c). (B) When maintained in log phase, incomplete scission during cell division produces chain-like colonies. Not shown: When grown with the bacterium *Algoriphagus machopogensis*, cells make compact rosette colonies (see SI). Scale bar: 10 μm

The choanoflagellate *Salpingoeca rosetta* uses a single whip-like flagellum to drive a flow of water and captures bacterial prey from the flow on a collar of microvilli. Although unicellular under many growth conditions, *S. rosetta* cultures maintained in log phase growth produce chain-like colonies bound together by extra-cellular matrix and cell-cell bridges [1, 2] (Fig. 1). Cells in colonies remain undifferentiated and divide autonomously. Because of *S. rosetta*'s phylogenetic position, and because its colonies lack many of the features of derived multicellularity, they are thought to share features in common with the progenitors of multicellular animals. Understanding the selective advantages of the colonial form may therefore reveal evolutionary and ecological forces that shaped the first origins of animal multicellularity.

The cooperative hydrodynamics of *S. rosetta* colonies cannot be described by existing theory for cooperative feeding. Using the Volvocales (a family of hollow spherical algal colonies) as a model system, Short *et al.* [3] showed flagellated cell-colonies increase nutrient uptake. The cells along the periphery of *Volvox* spp. colonies beat in a coordinated anterior-posterior direction to create an effective uniform propulsive stress, σ_s along the colony surface. The total propulsive force is balanced by viscous drag $\sim \eta R U_{\rm swim}$, with η the viscosity of the surrounding fluid, R the colony radius, and $U_{\rm swim}$ swimming-speed. If σ_s is conserved between colonies of different sizes, then $U_{\rm swim} \sim \sigma_s R/\eta$, so larger colonies swim faster and encounter more dissolved molecules or prey organisms per unit time.

By contrast, in colonial *S. rosetta* we find no evidence that flagellar phases, frequencies or axes are coordinated (SI and Supplementary Movie 1). Because flagella of different cells 'push' in different directions, forces from different parts of the colony tend to cancel and colonies swim more slowly and should feed less well than single cells. Here we identify another possible mechanism of hydrodynamic cooperation – showing that the anisotropically distributed cells of a colony create long range feeding flows, and draw in a larger volume flux of fluid per cell than cells can individually. Remarkably, slower swimming augments, rather than diminishes, the rate at which colonies draw in fluid.

S. rosetta prey encounter rates depend both on the speed of swimming of the organism and upon the dynamics of their flagella-created feeding flows. Typical flow Reynolds numbers are $\approx 10^{-4}$ [4], so viscous stresses are manyfold larger than inertial stresses [5]. The flow is therefore governed by Stokes' equations, and can be described completely by superposition of singularities, representing the action of point forces and sources [6].

A single point force accurately represents sessile choanoflagellate feeding flows. We used particle track-

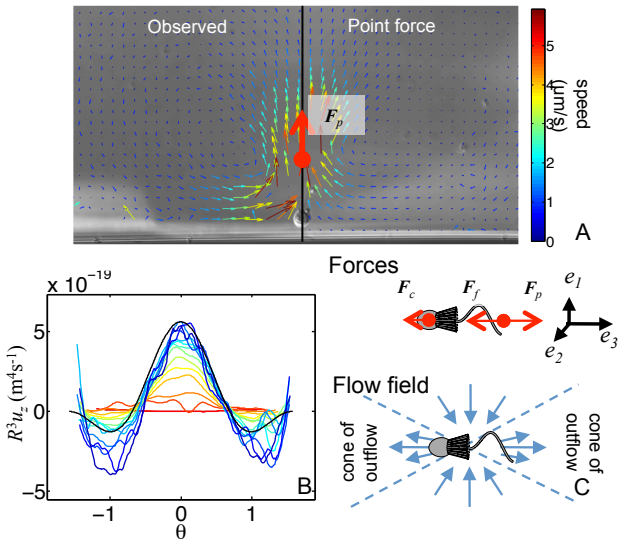

FIG. 2. Mapping and modeling feeding flows created by single *S. rosetta* cells. (A) Left panel: experimentally measured velocity field for a single thecate cell. 49000 bacterial velocity measurements were interpolated to a regularly-spaced grid of x,y points and then averaged over time. Arrows give displacements in 1s and are also color-coded by speed. Right panel: Flow field vectors from a point force model match the velocity field except adjacent to the cell body. (B) To determine the total flagellum force we match the measured velocity field far from the cell to the asymptotic form of the point force flow field. Colors: scaled velocity field $R^3 u_z$ on arcs of different radius (equispaced from red: $R = 12\mu$m to blue: $R = 74\mu$m), R, parameterized by polar angle θ. Black: theoretical velocity. (C) Upper panel: For a freely swimming cell, propulsive ($\boldsymbol{F}_p$) and drag forces ($\boldsymbol{F}_f$, $\boldsymbol{F}_c$) create a stresslet with principal axes $\{\boldsymbol{e}_i\}$ (upper panel), with cones of outflow (blue velocity arrows) fore and aft of the cell and inflow around the cell equator (lower panel).

ing [7] to analyze bacterial trajectories from videos (captured at 1 frame/s) of the flow produced by sessile (and therefore stationary) thecate *S. rosetta* cells anchored to cover-slides (Fig. 2A). We follow [4] by modeling the feeding flow as a constant point force, F_p, a distance h above the cover-slide, treated as an infinite planar surface [8]. We matched F_p and h from (i) the flow field, $\boldsymbol{u}$, far from the cell and (ii) the distance between cover-slide and the stagnation points. We found $F_p \equiv 2.4 \pm 0.8$ pN and that the point force is located 16.8±2.5 μm above the cell apex, coinciding approximately with the the flagellum tip. Although tailored to the far field velocities, this simplified model also quantitatively produces the velocity field close to the cell except near the base of the flagellum where neglect of the distributed flagellar force leads velocities to be underestimated (Fig. 2A)

Neglecting buoyancy, freely-swimming cells exert no net force on the surrounding fluid so the propulsive force $\boldsymbol{F}_p$ is balanced by drag forces on the cell body, $\boldsymbol{F}_c$, and flagellum, $\boldsymbol{F}_f$ [9]. We model these contributions by point forces located at $\boldsymbol{r}_p$, $\boldsymbol{r}_c$ and $\boldsymbol{r}_f$ respectively (Fig 2C), identifying $\boldsymbol{r}_c$ with the center of the cell body, and $\boldsymbol{r}_f = \boldsymbol{r}_p$ as the flagellum tip. Then, at a point $\boldsymbol{r}$, far from the cell, the forces resolve into the stresslet flow field $\boldsymbol{u} = -\frac{3(\boldsymbol{r}\cdot\boldsymbol{S}\cdot\boldsymbol{r})\boldsymbol{r}}{8\pi\eta r^5}$ where:

$$\boldsymbol{S} = -\sum_{i\in\{p,c,f\}} \left[\frac{1}{2}\left(\boldsymbol{F}_i\boldsymbol{r}_i + \boldsymbol{r}_i\boldsymbol{F}_i\right) - \frac{1}{3}\left(\boldsymbol{r}_i\cdot\boldsymbol{F}_i\right)\mathbf{1}\right], \quad (1)$$

($\mathbf{1}$ is the identity tensor). We estimate the drag forces by resistive force theory [10]: Specifically, if $\boldsymbol{U}$ is the swimming speed and $\boldsymbol{n} = (\boldsymbol{r}_f - \boldsymbol{r}_c)/||\boldsymbol{r}_f - \boldsymbol{r}_c||$ is a unit vector in the direction of the flagellum then $\boldsymbol{F}_c = 6\pi d\eta\boldsymbol{U}$ ($d = 2.4\mu$m for radius of the cell) and $\boldsymbol{F}_f = (Z_\parallel - Z_\perp)(\boldsymbol{U}\cdot\boldsymbol{n})\boldsymbol{n} + Z_\perp\boldsymbol{U}$ (see SI for derivation of the drag coefficients $Z_\parallel$ and $Z_\perp$). Balance of forces, $\sum_{i\in\{p,c,f\}}\boldsymbol{F}_i$, then yields $U = \frac{F_f}{6\pi\eta d + Z_\parallel} = 28\mu\text{ms}^{-1}$ comparable with measured swimming speeds (M. Koehl, N. King, and R. Stocker, unpubl.) and also the values of the forces $\boldsymbol{F}_{c,f}$.

The stresslet flow continuously supplies fresh fluid, undepleted of prey bacteria, to the cell. The stresslet tensor $\boldsymbol{S}$ is symmetric and traceless so can be diagonalized by an orthonormal basis of eigenvectors: $\boldsymbol{e}_i$ $i = 1, 2, 3$, with eigenvalues λ_i: $\sum_i \lambda_i = 0$. Two of the eigenvalues, λ_1 and λ_2 say, must have the same sign. If $\lambda_3 > 0$, there is radial inflow inside of a pair of elliptical cones with axes on $\pm\boldsymbol{e}_3$ and radial outflow outside of these cones. Flow in the two regions is reversed if $\lambda_3 < 0$. Assuming $|\lambda_1| \geq |\lambda_2|$ we can compute the fluid flux over any surface enclosing the swimmer to obtain the rate of fluid supply through the cones of inflow:

$$f = \frac{|\lambda_1|^{5/2}}{3\pi\eta|\lambda_1 - \lambda_3|^{3/2}}\left|M_{5/2,3/2} - 3\left(1 - \frac{\lambda_3}{\lambda_1}\right)M_{3/2,1/2} - \frac{\lambda_3}{\lambda_1}M_{3/2,3/2}\right| \quad (2)$$

where $M_{p,q} \equiv \int_0^{\pi/2} \frac{(1-r\sin^2\phi)^p}{(1-s\sin^2\phi)^q}\,d\phi$ for $r \equiv \frac{\lambda_1-\lambda_2}{\lambda_1}$, $s \equiv \frac{\lambda_1-\lambda_2}{\lambda_1-\lambda_3}$ (see SI for more details). Though the terms in (2) must in general be evaluated by numerical quadrature if (i) $|\lambda_1| \gg |\lambda_2|$ then $f \sim \frac{|\lambda_1|}{\pi\eta}$ or (ii) $\lambda_1 \approx \lambda_2$ then $f \sim \frac{|\lambda_1|}{3^{1/2}\pi\eta}$. In general the flux to the cell increases in proportion to the largest eigenvalue of $\boldsymbol{S}$ i.e. increases with the size of the forces or their separation.

If cells swim at velocity $\boldsymbol{U}$ then fluid is also advected to the cell at rate $f_{\text{adv}} = \pi R^2 U$, where R is the radius of a spherical control surface. For a single swimming cell the modeled values of f and U give $f_{\text{adv}}/f = 0.02R^2$, if R is measured in μm. Thus at large distances, advection dominates but within $\sim 7\,\mu$m of the cell, transport is dominated by the stresslet flow: swimming faster does not increase the total flux (see SI). Colonies will be shown to swim slower and have larger stresslet eigenvalues, so the stresslet flow field dominates up to even greater distances.

Pairs of choanoflagellate cells anchored together can access a greater volume of new fluid per unit time than freely-swimming cells. We modified our model to include the effect of two cells swimming together: Cell dimers are developmental and evolutionary intermediates between individual cells and chain-like colonies. Dimer configurations are specified by three angles: θ_1 is the smallest angle between the flagellum of the first cell and the normal to the axis joining the two cell centers and (θ_2, ϕ_2) are the spherical polar angles of the second flagellum relative to the normal vector. (Fig. 3A). $(\theta_1, \theta_2, \phi_2)$ are set during cell-division by the position of the cell-cell bridge and direction of the polarity axis of the daughter cell. A cell-dimer is associated with 6 point forces, $\{\boldsymbol{F}_i^j : i \in \{p, c, f\},\ j \in \{1, 2\}\}$(Fig. 3B). For any general arrangement of these forces, the dimer will rotate with angular velocity $\boldsymbol{\Omega}$ and will swim with velocity $\boldsymbol{U}$, determined by the condition that the dimer be force and torque free. For each pair (θ_1, θ_2), we determine ϕ_2 to maximize f (Fig. 3C).

The flower-like shape of the (θ_1, θ_2, f) surface reveals two locally optimal configurations for a pair of cells; pole-to-pole or side-by-side (Fig 3C) with fluid fluxes per cell that are respectively 2.17× larger and identical to freely swimming cells. Pole-to-pole configurations increase the stresslet eigenvalues for two reasons: First slower swimming (Fig. 3C) increases the flagellar force $\boldsymbol{F}_p^i + \boldsymbol{F}_f^i$ by reducing the drag forces acting on individual flagella, mimicking the observed increase in fluid transport by the flagellum of a cell prevented from swimming [11, 12]. Second, the separation of the two flagellar forces $\boldsymbol{F}_p^{\{1,2\}}$ is maximized.

We extended our calculations to chain-like colonies of more than two cells. If cells independently regulate their positions then N-cells have $4N - 5$ configurational degrees of freedom. However, tuning of these parameters during colony morphogenesis requires information to be propagated between cells, since the division of any cell alters the position of all of the other cells within the chain. We therefore apply a simple morphogenetic model: For $i = 1, 2, \ldots N - 1$, we use the landmarks of the cell i (flagellum direction $\boldsymbol{n}_i$, displacement $\boldsymbol{r}_c^i - \boldsymbol{r}_c^{i-1}$ from cell $(i - 1)$) to define coordinate axes. We require that each cell division be identical: i.e. the coordinates of the flagellum vector $\boldsymbol{n}_{i+1}$ and displacement $\boldsymbol{r}_c^{i+1} - \boldsymbol{r}_c^i$ of the $(i + 1)-$th cell be independent of i with respect to these axes. This model has the advantage that any cell-division occurring in a N-cell colony produces the same $N + 1$ cell colony, independently of which cell divided. Chains formed by this rule are helices with constant curvature and torsion. The four degrees of freedom in cell position and orientation dictate the curvature κ and torsion τ of the helix and the flagella angles relative to the tangent, normal and binormal of the helix. Given N, κ and τ we choose the orientational angles of the flagella in the colony to optimize f (Fig 4A-C). When $N = 3$, the optimal configuration has $(\kappa, \tau) = (1/d, 1/d)$, the largest values compatible with the finite size of cells: cells are stacked almost side by side, their flagella lying in parallel planes and pointing toward the vertices of an equilateral triangle, per-cell fluid supply is 75% greater than for freely-swimming cells (Fig 4A). As N increases, the optimal helix becomes a semi-circular arc with flagella pointing radially outward (Fig 4A-C), similar to real *S. rosetta* colonies (Fig 1B).

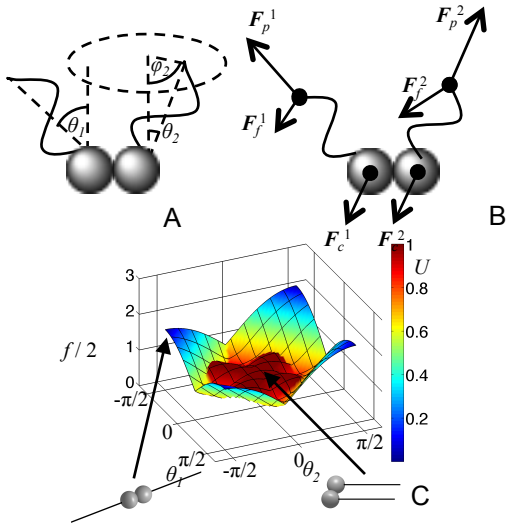

FIG. 3. Enhanced feeding in dimers of *S. rosetta* cells. (A) We measured how the volume flux of fluid to the cells in the dimer, f, depends upon the orientations of the two cells, parameterized by angles $(\theta_1, \theta_2, \phi_2)$. (B) To compute the feeding flux, we balance the propulsive forces $\boldsymbol{F}_p^{1,2}$ from the two cells with drag forces $\boldsymbol{F}_{c,f}^{1,2}$ from the cell bodies and flagella. To do this we must also obtain the swimming and rotational velocities $(\boldsymbol{U}, \boldsymbol{\Omega})$ of the cell-dimer. (C) Feeding flux, non-dimensionalized by the total flux to two cells feeding individually, for different configurations of cells. Here we vary (θ_1, θ_2) and for each such pair of angles select the value of ϕ_2 to maximize f. f is non-dimensionalized by f_{single}, flux for a single freely-swimming cell; $f/2 > 1$ means that the volume flux per cell is greater than for freely-swimming cells. Surface-coloring shows the swimming speed of the dimer U, non-dimensionalized by the swimming speed of a single cell. Pole-to-pole $(\theta_1, \theta_2) = (\pm\pi/2, \pm\pi/2)$ and side-by-side $(\theta_1, \theta_2) = (0, 0)$ configurations are shown.

Do the volume fluxes increase in proportion to the number of cells in the chain? We analyzed the fluid supply to a large semicircle of N cells (see SI for detailed calculations), and found using real *S. rosetta* dimensions that $f \sim 65N^2 \mu\text{m}^3\text{s}^{-1}$, increasing faster than the colony's metabolic needs ($\sim N$).

We measured the angles between the axes of neighboring cells in real choanoflagellate colonies (Fig. 5A). Average cell-cell angles were relatively conserved between colonies (mean: 0.60±0.17 rads for *S. rosetta*). Although intra-colony variation in cell-cell angles (mean: 0.22 ra-

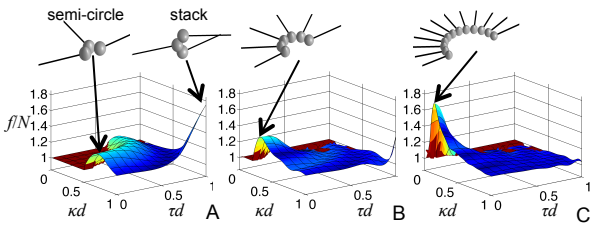

FIG. 4. Optimal helical cell configurations. (A) For three cells, the optimal helix is a stack, while an additional, local optimum is formed from a semicircular arc of cells with flagella pointing in an outward radial direction. (B-C) For $N = 6$ and $N = 12$ cells the semi-circular arc becomes the optimal helix.

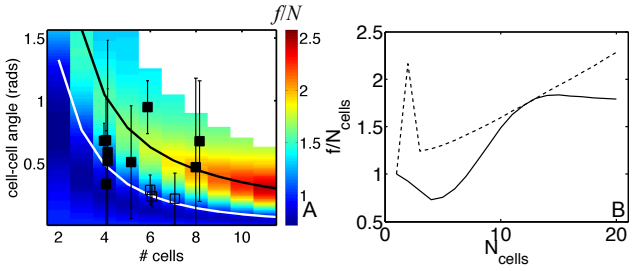

FIG. 5. (A) Cell-cell angles measured from real chain colonies of *S. rosetta* (■) cultured and imaged using standard techniques [2], and *Desmarella* cf. *moniliformis* (□) [13]. Error bars: s.d. Cell numbers are slightly displaced from integer values for clarity. Heat map gives the predicted per-cell flux f/N. White line: minimum cell-cell angle for $f/N > 1$, grey line: optimal cell-cell angle for a semicircular colony.(B) We simulated feeding by developmental precursors of a colony with $N = 12$ cells (solid curve). Intermediate-sized colonies feed less well even than freely swimming cells ($f/N < 1$ for $N < 8$), and much worse than semicircular colonies (dashed curve).

dians) reduces f/N, the variation is small enough that $f/N > 1$ (see SI). Mean cell-cell angles did not depend on colony size, suggesting that chains conserve their curvature during growth. Although $f/N > 1$ for each colony, most observed colonies were far from the optimal helical geometry for their size (Fig. 5A). Hypothesizing that fixing cell-cell angles would produce suboptimal values of f/N at some stage in colony development, we simulated growth of a colony with $N = 12$ cells. We chose cell-cell angles to maximize f for $N = 12$. Intermediate colonies with these cell-cell angles have smaller per-cell fluid supply f/N (Fig. 5B) than colonies with optimal helical geometry. In fact, over most of its development (for $N < 8$) $f/N < 1$, so colonies fed worse even than single cells. Colonies grown beyond 12 cells did relatively less well than the optimal helical colonies for each cell number (Fig. 5B). These data suggest that cell-cell angles in real colonies may be constrained by trade-offs between maximizing feeding rates at earlier and later growth stages.

Our modeling predictions suggest that cooperative hydrodynamics may offer a competitive advantage to modern colonial choanoflagellates and the early metazoans they are believed to resemble [14]. Decreased drag forces upon flagella and greater spatial separation of flagella forces increase the colony stresslet and its supply of fresh fluid. If enhanced feeding by cooperative hydrodynamics were an evolutionary force toward multicellularity, there are constraints on the configurations and numbers of cells involved. However, we also find that a simple morphogenic model is sufficient to produce such configurations without requiring cell-cell communication or coordination of flagellar beating.

Although fresh fluid supply provides an upper bound upon the rate at which prey is drawn to the colony and is a common proxy for feeding rate [11, 15], colonies of different sizes and freely-swimming single cells may differ in their abilities to remove prey from these flow fields. Full validation of the model will require either direct imaging [16] or simulations [17] of prey capture by both single and colonial cells.

Why does S. rosetta have unicellular as well as multicellular forms? Real prey distributions are patchy [18] and successful flagellar feeders must forage for and exploit prey patches. Colonies swim slower than single cells so are disadvantaged moving between prey patches. Since colony formation is triggered when cells are maintained with high concentrations of bacterial prey we hypothesize that colonies may be a transient life-phase triggered when *S. rosetta* cells find themselves in persistent patches.

We gratefully acknowledge financial support from the Alfred P. Sloan Foundation (to MR), from the Miller Institute for Basic Research (to MR, MD and REP), and from the National Science Foundation (grant #IOS-1147215) to MK.

[1] S. Fairclough, M. Dayel, and N. King, Curr. Biol., **20**, R875 (2010).
[2] M. J. Dayel, R. A. Alegado, S. R. Fairclough, T. C. Levin, S. A. Nichols, K. McDonald, and N. King, Dev. Biol., **357**, 73 (2011).
[3] M. Short, C. Solari, S. Ganguly, T. Powers, J. Kessler, and R. Goldstein, Proc. Nat. Acad. Sci USA, **103**, 8315 (2006).
[4] M. Pettitt, B. Orme, J. Blake, and B. Leadbeater, Eur. J. Protistol., **38**, 313 (2002).
[5] E. Purcell, Am. J. Phys, **45**, 3 (1977).
[6] S. Kim and S. J. Karrila, *Microhydrodynamics: Principles and selected applications* (Butterworth-Heinemann, 1991).
[7] J. Crocker and D. Grier, J. Coll. Int. Sci., **179**, 298 (1996); M. Roper, A. Simonin, P. Hickey, A. Leeder, and N. Glass, "Nuclear dynamics in a fungal chimera," (2012), submitted to Proc. Nat. Acad. Sci. USA.
[8] J. Blake, Proc. Camb. Phil. Soc, **70**, 303 (1971).

[9] T. Pedley and J. Kessler, Ann. Rev. Fluid Mech., **24**, 313 (1992); K. Drescher, J. Dunkel, L. H. Cisneros, S. Ganguly, and R. E. Goldstein, Proc. Nat. Acad. Sci. USA, **108**, 10940 (2011).
[10] J. Gray and G. Hancock, Journal of Experimental Biology, **32**, 802 (1955); C. Brennen and H. Winet, Ann. Rev. Fluid Mech., **9**, 339 (1977); M. Roper, R. Dreyfus, J. Baudry, M. Fermigier, J. Bibette, and H. A. Stone, J. Fluid Mech., **554**, 167 (2006).
[11] K. Christensen-Dalsgaard and T. Fenchel, Aquat. Microb. Ecol., **33**, 77 (2003).
[12] J. Lighthill, SIAM Review, **18**, 161 (1976).
[13] "The encyclopedia of life," URL: www.eol.org, retrieved on 01 Feb. 2013.
[14] N. King, Dev. Cell, **7**, 313 (2004).
[15] S. Childress, M. Koehl, and M. Miksis, J. Fluid Mech, **177**, 407 (1987).
[16] T. Fenchel, Limnol. Oceanogr., 733 (1980).
[17] L. Fauci, Am. Zool., **36**, 599 (1996).
[18] J. P. Barry and P. K. Dayton, in *Ecological Heterogeneity*, Ecological Studies, Vol. 86, edited by J. Kolasa and S. Pickett (Springer, 1991) pp. 270–320.